Catalysis Science & Technology

Accepted Manuscript

ROYAL SOCIETY OF CHEMISTRY

www.rsc.org/catalysis

Journal Name

ARTICLE

Styrene hydrogenation performance of Pt nanoparticles with controlled size prepared by atomic layer deposition

Received 00th January 20xx,
Accepted 00th January 20xx

DOI: 10.1039/x0xx00000x

www.rsc.org/

Jianwei Li,[a,b] Bin Zhang,[b] Yao Chen,[b,c] Jiankang Zhang,[b] Huimin Yang,[b] Jiwen Zhang,[d] Xiaoli Lu,[d] Guicun Li,[a,*] Yong Qin[b,*]

Highly dispersed Pt sub-nanoparticles supported on carbon nanotubes (CNTs) with well controlled size have been prepared by atomic layer deposition. Their particle size distribution was characterized by TEM. The obtained Pt sub-nanoparticles exhibit unusual catalytic performance for styrene hydrogenation. It is revealed that the turnover frequency (TOF) of the Pt/CNTs catalysts for this reaction is well correlated with the Pt particle size. The highest TOF was obtained with a Pt/CNTs catalyst having an average Pt particle size around 0.5-0.7 nm.

1. Introduction

Supported Pt nanoparticles are proven catalysts for a variety of chemical processes such as direct methanol fuel cells,[1,2] proton exchange membrane fuel cells,[3] the selective partial hydrogenation,[4] direct hydrogenation of nitrobenzene to aniline under mild conditions,[5] visible-light-induced photocatalytic hydrogen generation[6] and oxygen reduction reaction.[7] The improvement of metal dispersion will lead to higher activity and selectivity for supported catalysts.[8,9] For example, the product selectivity and turnover rate for furfural decarbonylation/hydrogenation reaction can be well controlled by the size and shape of Pt nanoparticles.[10] Recent study suggests that sub-nanometer metal particles commonly exist in supported catalysts and play an important role in catalytic activity.[11-13] Downsizing of Pt nanoparticle to cluster or even single atom could significantly increase their catalytic activity.[14,15] Pt nanoclusters (0.8 nm) supported on graphene are expected as excellent electro-oxidation catalysts.[12] However, the large-scale synthesis of practical and stable clusters and atoms remains a significant challenge because sub-nanoparticles are prone to aggregation under reaction conditions. Therefore, the hydrogenation performance of Pt sub-nanoparticles is rarely reported due to the difficulty of obtaining highly uniform sub-nanoparticles via traditional methods.

Atomic layer deposition (ALD) is proved to have the capability of precise control over particle size from single atom, nanocluster, to nanoparticle.[14,16,17] In ALD process, a substrate is alternately exposed to different reactive precursor vapours to deposit materials in an atomic layer-by-layer fashion. Previous studies have revealed the controllable morphology of deposited metal and metal oxides in atomic scale by ALD.[14,17] ALD has outstanding advantages to create and modify various catalytic structures in atomic scale, such as high surface area oxides, metal nanoparticles,[14] bimetallic nanoparticles,[16,18] core-shell nanostructures,[19] and controlled microenvironments[20] etc.

Carbon nanotubes (CNTs) are promising materials in various fields due to their unique mechanical, chemical, and electrochemical properties.[21,22] CNTs have been widely used as support materials for heterogeneous catalysts.[23] In general, CNTs are pre-treated with strong oxidants to create functional surface groups (–OH,–COOH and>C=O).[4,24,25] These oxygen-containing surface groups will anchor metal precursors or nanoparticles to improve their dispersion on CNTs.[26,27] However, the nanoparticles supported on CNTs are prone to deactivation due to aggregation, growth of particle size and change in shape.[28,29] It is still a big challenge to improve the durability of metal nanoparticles supported on CNTs, in particular, sub-nanoparticles.

In this study, we developed a simple route to prepare sub-nanometer Pt particles with uniform dispersion supported on CNTs by ALD. The size of Pt nanoparticles can be precisely controlled by varying the number of ALD cycles. The sub-nanometer size effect of Pt particles less than 1 nm was studied in hydrogenation of styrene.

2. Experimental Section

2.1. The Pretreatment of CNTs

CNTs with a special surface area of 130~160 m^2/g and diameter of 40~60 nm were bought from Shenzhen Nanotech Port Co.. Before Pt ALD, the CNTs were typically treated in

[a] College of Materials Science and Engineering, Qingdao University of Science and Technology, Qingdao, 266042, PR China, guicunli@qust.edu.cn
[b] State Key Laboratory of Coal Conversion, Institute of Coal Chemistry, Chinese Academy of Science, Taiyuan 030001, PR China, qinyong@sxicc.ac.cn.
[c] Graduate University of Chinese Academy of Sciences, Beijing 100039, PR China
[d] State Key Discipline Laboratory of Wide Band Gap Semiconductor Technology, School of Microelectronics, Xidian University, 710071 Xi'an, China
† Footnotes relating to the title and/or authors should appear here.
Electronic Supplementary Information (ESI) available: [details of any supplementary information available should be included here]. See DOI:10.1039/x0xx00000x

concentrated nitric acid at 120 °C under refluxing conditions for 6 h to remove impurities and create oxygen-containing groups. Then the CNTs were thoroughly washed with distilled water and ethanol three times and dried at 110 °C.

2.2. Catalyst Preparation

ALD process was carried out in a home-made, hot-wall, closed-chamber type ALD reactor, utilizing N_2 as carrier gas. The Pt sub-nanoparticles were deposited by sequential exposure of the CNTs substrates to (methylcyclopentadienyl)trimethylplatinum ($MeCpPtMe_3$) and O_3. The deposition temperature was 300 ^oC, and $MeCpPtMe_3$ was kept at 60 ^oC. The pulse, exposure, and purge times for $MeCpPtMe_3$ precursor were 0.5, 10, and 20 s, and those for O_3 were 1, 10, and 20 s, respectively. Pt/CNTs catalysts with different Pt particle sizes were obtained by varying the cycle numbers of ALD growth. In this paper, we prepared five different Pt/CNTs catalysts with cycle numbers of 1, 2, 5, 8 and 10 for Pt deposition (designated as PtX/CNTs with X indicating the number of ALD cycles), respectively.

2.3. Characterization

The particle size and distribution of these catalysts were analyzed on a JEOL-2100F microscope. The elemental composition of these catalysts was investigated using energy dispersive X-ray spectroscopy (EDS) under the electron microscope. Pt loading of the samples was obtained by optical emission spectroscopy with inductive coupling plasma (ICP-OES) using a Thermo iCAP6300 equipment. Fourier transform infrared spectroscopy (FTIR) was carried out using a Bruker Tensor 27 instrument at a resolution of 4 cm^{-1} with 200 scans for each sample. Raman spectra were collected with a Labram HR800 (Horiba Jobin Yvon, Palaiseau, France) spectrometer employing a He–Ne laser with an excitation wavelength of 514nm. X-ray photoelectron spectra (XPS) were recorded on an ES-300 photoelectron spectrometer (KRATOS Analytical) with an Al Kα source (1486.6 eV). The Pt/CNTs catalysts were pre-treated in H_2/N_2 at 353 K for 2 h before XPS analysis. Platinum dispersion was determined by hydrogen titration of chemisorbed oxygen in a Xianquan TP-5080 multi-functional automatic adsorption instrument with a thermal conductivity detector. Before hydrogen titration, the catalysts (50-120 mg) were pre-treated under H_2-N_2 mixtures at 473 K for 30 min, purged under N_2 for 30 min and then cooled to 393 K. Oxygen was introduced to pre-adsorb on Pt surface at 393 K, purged under N_2 for 30 min and then cooled to 323 K. Hydrogen titration of chemisorbed oxygen (N_2 as carrier at 30 mL min^{-1}) was performed at 323 K using an injection loop of 1 mL and pulse of 10% H_2/N_2 mixture injected every 2 min to investigate the number of Pt surface active sites.

2.4. Activity measurement

Catalyst performance was tested in an autoclave with a capacity of 25 mL, which contained 5 mg catalyst, 0.9 g styrene as reactant and 10 mL isopropanol as solvent. The hydrogenation reactions were carried out at room temperature under 3 MPa H_2 pressure with stirring. The conversion of styrene was detected by gas chromatography equipped with a hydrogen flame ionization detector (FID).

3. Result and discussion

3.1 Characterization of Pt catalysts

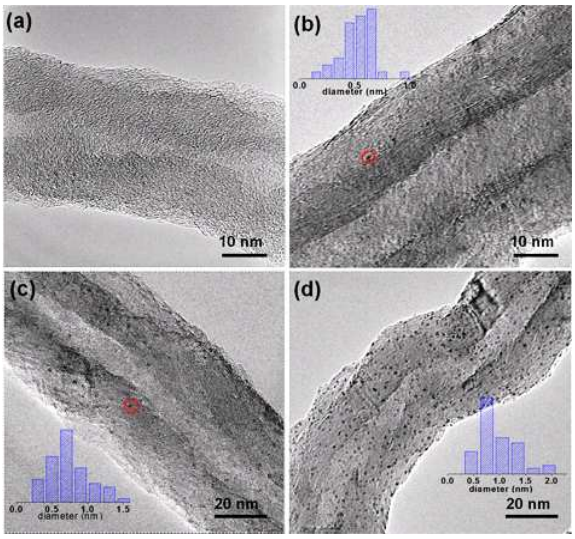

Figure 1. TEM images of the Pt/CNTs catalysts prepared by ALD: (a) Pt2/CNTs, (b) Pt5/CNTs, (c) Pt8/CNTs and (d) Pt10/CNTs.

The morphology and particle size distribution of the catalysts are shown in the TEM images (Figure 1). The corresponding size distribution histograms are also presented. Pt nanoparticles are not clearly visible for the Pt1/CNTs and Pt2/CNTs samples (Figure 1a), possibly because the particle size is too small (cluster) or exist in the form of single atom[30]. Pt particle size increases with the increase of cycle number of Pt ALD. The average particle size ranges from 0.5 nm (5 cycles) to 0.9 nm (10 cycles) with a narrow size distribution.

EDS and ICP-OES analyses were performed for all catalysts to examine the elemental composition and Pt loading. Figure 2(a) reveals the presence of C, O and Pt elements in the samples. The existence of O element is possibly resulted from the oxygen-containing functional groups on the surface of CNTs. Figure 2(b) suggests that the content of Pt increases linearly with the number of deposition cycles. The Pt loading increases with about 0.3 wt% and 0.23 wt% per ALD cycle from EDS and ICP analyses, respectively. The difference between EDS and ICP results is because EDS is a semiquantitative analysis technique.

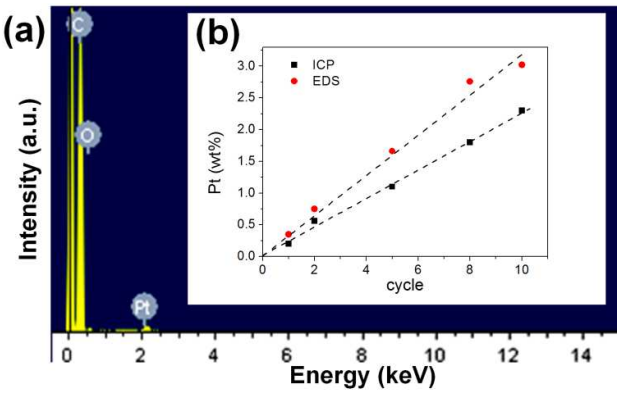

Figure 2. (a) EDS spectrum and (b) Pt contents as a function of the ALD cycle number.

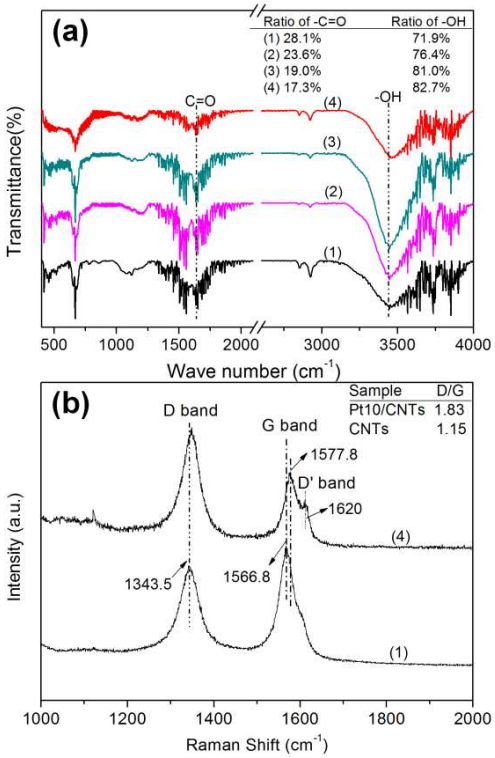

Figure 3. FTIR (a) and Raman (b) spectra of different samples: (1) HNO_3 treated CNTs, (2) CNTs treated with 10 ALD cycles of O_3, (3) Pt1/CNTs, and (4) Pt10/CNTs.

FTIR and Raman analyses are performed to detect the overall change of functional groups and defects of CNTs surface before and after ALD process. For comparison, FTIR analysis was also conducted for CNTs treated with 10 cycles of O_3 (without Pt precursor). As shown in Figure 3(a), the acid treated CNTs exhibits two prominent adsorption bands centred around 1647.5 and 3440.7 cm^{-1}, which can be assigned to the stretching vibration of C=O and -OH , respectively.[31-34] The ratio of –OH to –COOH contents increases after O_3 treatment. It also increases with the cycle number of Pt ALD. This may be due to the generation of –OH group and/or the oxidation of –COOH group during Pt ALD. The intensities of the C=O and –OH are dramatically decreased for Pt10/CNTs, suggesting the consumption of surface groups of CNTs during Pt ALD. The weak peaks at 2930 cm^{-1} and 2860 cm^{-1} are attributed to the C-H stretching vibration on the surface of CNTs. The C-H species are obviously weakened for O_3-treated CNTs and Pt/CNTs, suggesting the oxidation of C-H species on CNTs surface. The Raman spectra of CNTs and Pt10/CNTs were shown in Figure 3(b). The two bands around 1340 cm^{-1} (D band) and 1580 cm^{-1} (G band) are the main features of the CNTs structure for both samples. The small shoulder peak at around 1620 cm^{-1} is described as the D' band which can be observed obviously in Pt10/CNTs sample. The G band peak of Pt10/CNTs shifts by 11 cm^{-1} to a higher wavenumber compared with that of CNTs. The specific value of D/G calculated from peak area increase from 1.15 to 1.83, indicating that a large amount of defects are produced on the CNTs surface after Pt ALD. This can be attributed to the oxidation of surface of CNTs by O_3 during the ALD deposition, and the catalytic effect of Pt nanoparticles deposited on CNTs to promote the oxidation process.[35]

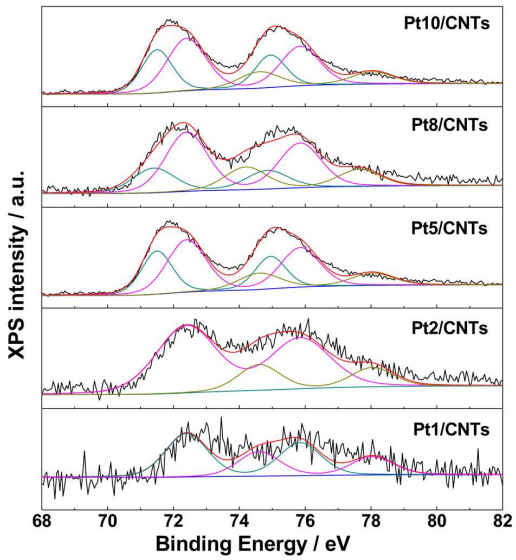

Figure 4. X-ray photoelectron spectra of Pt4f levels for the prepared Pt/CNTs catalysts.

Table 1. Summary of XPS results for Pt4f.

Catalyst	Binding energy (eV)	FWHM (eV)	% relative intensities	Assignment
Pt1/CNTs	72.4	1.5	64.1	Pt^{2+}
	74.6	1.5	35.9	Pt^{4+}
Pt2/CNTs	72.4	2.1	78.9	Pt^{2+}
	74.6	1.5	21.1	Pt^{4+}
Pt5/CNTs	71.4	1.5	7.4	Metallic Pt
	72.4	1.5	56.4	Pt^{2+}
	74.2	2.0	36.2	Pt^{4+}
Pt8/CNTs	71.4	1.5	23.1	Metallic Pt
	72.4	1.5	55.6	Pt^{2+}
	74.2	1.5	16.9	Pt^{4+}
Pt10/CNTs	71.5	1.1	32.7	Metallic Pt
	72.4	1.4	50.4	Pt^{2+}
	74.6	1.5	16.9	Pt^{4+}

3.3 XPS analysis of Pt/CNTs catalysts

The electronic state of Pt for Pt/CNTs catalysts was investigated by XPS (Figure 4). It is well established that particle morphology and size have significant impact on the electronic properties of nanoparticles. The Pt4f binding energy in Pt/CNTs significantly shifts (by 0.7 eV) to a lower energy with the increase of ALD cycle number. This shift value is similar to that of Pt4f from bulk state to isolated Pt atoms, which was attributable to the final-state effect in the Pt4f core level.[36] Table 1 summarizes the BE, FWHM and the relative intensities of all the Pt species and their assignment. The existence of the peak at 71.4-71.5 eV is attributed to metallic Pt^0 species, and the other two peaks at 72.4–72.6 eV and at 74.2–74.6 eV are attributed to platinum atoms in the 2+ and 4+ oxidation states, respectively.[37-39] The XPS analysis shows that Pt1/CNTs and Pt2/CNTs catalysts consist only oxidized Pt species (such as Pt^{2+}, Pt^{4+}) while Pt5/CNTs, Pt8/CNTs and Pt10/CNTs catalysts comprise metallic Pt^0 species. The relative intensity of metallic Pt^0 on Pt/CNTs increases with the increase of Pt particle size.

3.2 Catalytic performance

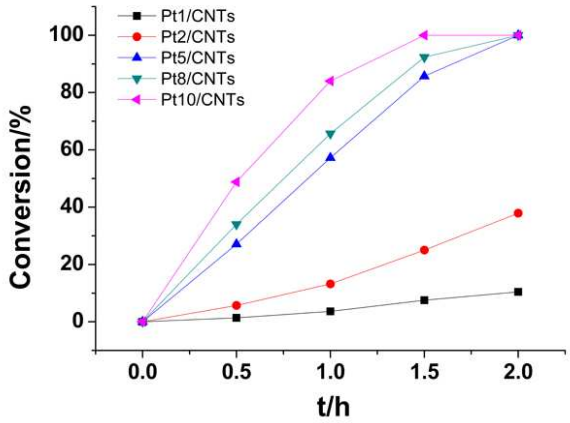

Figure 5. Conversion of styrene hydrogenation with Pt/CNTs prepared using different ALD cycle numbers for Pt deposition. Reaction conditions: 5 mg of catalyst, 0.9 g of substrate, 3 MPa H_2, and 298 K.

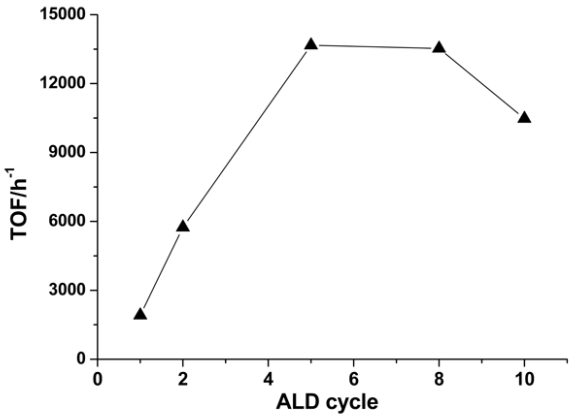

Figure 6. TOF of styrene hydrogenation with Pt/CNTs prepared using different ALD cycle numbers for Pt deposition.

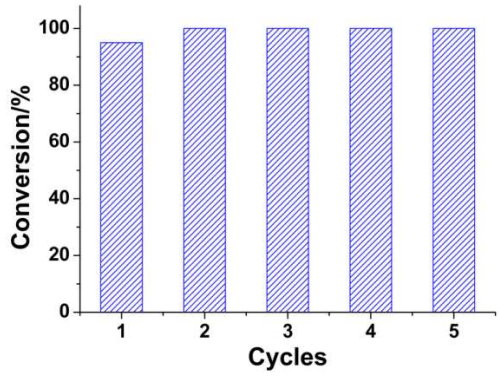

Figure 7. Reusability of Pt5/CNTs for styrene hydrogenation.

The conversion of styrene hydrogenation over Pt/CNTs catalysts with different ALD cycle numbers was plotted as a function of reaction time. As shown in Figure 5, the conversion increases with the increase of reaction time and ALD cycle numbers. There is a noticeable improvement in the hydrogenation rate with the increase of Pt content. To further confirm the intrinsic activity of Pt sub-nanoparticles on CNTs, the initial turnover frequency (TOF) value (0.5 h) of the catalysts with different Pt ALD cycle numbers is calculated and (Figure 6). The initial TOF values of Pt5/CNTs, Pt8/CNTs and Pt10/CNTs catalysts are apparently higher than those of Pt1/CNTs and Pt2/CNTs. It is clear that the Pt5/CNTs catalyst exhibits the highest TOF value. Pt8/CNTs catalysts exhibit nearly the same TOF in styrene hydrogenation. Further increasing the ALD cycle number induces a decline of the TOF value. TEM results show that the particle size of Pt supported on CNTs becomes larger with the increase of the ALD cycle numbers. Therefore, the TOF has a strong dependence on the Pt particle size. XPS results suggest that the increase of particle size induces the change of Pt surface electron density. The Pt1/CNTs and Pt2/CNTs only have the electropositive Pt species (Pt^{2+} and Pt^{4+}). Metal Pt species appeared for over five ALD cycles, and its content increases with the increase of Pt particle size. Thus, metal Pt^0 species is the main active site in styrene hydrogenation, because Pt1/CNTs and Pt2/CNTs show lower TOF than Pt5/CNTs, Pt8/CNTs and Pt10/CNTs. However, the TOF does not further increase with the content of metal Pt^0 species. Therefore, the electropositive Pt species can also influence the catalytic activity. The synergy of metallic and oxidized Pt species highly dispersed on the surface of CNTs has a particular electronic state, which is more effective for catalytic oxidation-reduction reaction and results in the highest activity for Pt5/CNTs and Pt8/CNTs catalysts.

The reusability of Pt5/CNTs for styrene hydrogenation was tested (Figure 7). A slightly increase in the catalytic activity was observed for Pt5/CNTs catalyst after the first experiment due to the reduction and activation of Pt particles by H_2. The styrene conversion of Pt5/CNTs still remains 100% even after five repeating experiments. FTIR spectra reveal that the content of surface –OH and C=O bond are decreased after ALD deposition. Raman spectra reveal that the ALD process introduces more surface defects on CNTs. These surface defects can improve the interaction between the sub-nanoparticles and the CNTs.[40,41] Therefore, Pt sub-nanoparticles with high surface energy can stay stably on the surface of CNTs. This research on styrene hydrogenation using Pt sub-nanoparticles will promote the design of high efficiency Pt catalysts.

Conclusion

ALD was used to control the size of Pt sub-nanoparticles supported on CNTs. Pt particle size is closely related to the platinum loading which increase linearly with the ALD cycle number. It is a promising model system for evaluation of the effect of sub-nanometer particle and surface structure in styrene hydrogenation. The Pt5/CNTs and Pt8/CNTs with a particle diameter around 0.5-0.7 nm exhibit the highest TOF compared to other catalysts. XPS measurement reveals that Pt/CNTs contain surface atoms in Pt^0, Pt^{2+} and Pt^{4+}, while only the samples with a particle size larger than 0.5 nm contain metallic Pt species. The modification of the electronic properties may be responsible for the enhanced catalytic performance. g FTIR and Raman analyses reveal the strong interaction between the Pt particles and the surface defects, which results in good stability. ALD has the potential to study the relation between the catalyst performance and the catalyst structure in a sub-nanometer scale.

Acknowledgments

We appreciate the financial supports from the National Natural Science Foundation of China (21403272, 21403271, 21203229, 21173248, and 51202176), the Hundred Talents Program of the Chinese Academy of Sciences, the Hundred Talents Program of Shanxi Province, Natural Science Foundation of Shanxi Province (2014011012-1), the Projects of the State Key Laboratory of Coal Conversion of China (2014BWZ004).

Notes and references

1. Y. Y. Mu, H. P. Liang, J. S. Hu, L. Jiang and L. J. Wan, *J. Phys. Chem. B*, 2005, **109**, 22212-22216.
2. Y. H. Lin, X. L. Cui, C. Yen and C. M. Wai, *J. Phys. Chem. B*, 2005, **109**, 14410-14415.
3. K. Lee, J. Zhang, H. Wang and D. P. Wilkinson, *J. Appl. Electrochem.*, 2006, **36**, 507-522.
4. V. Lordi, N. Yao and J. Wei, *Chem. Mater.*, 2001, **13**, 733-737.
5. C.-H. Li, Z.-X. Yu, K.-F. Yao, S.-f. Ji and J. Liang, *J. Mol. Catal. A: Chem.*, 2005, **226**, 101-105.
6. Q. Y. Li, L. A. Chen and G. X. Lu, *J. Phys. Chem. C*, 2007, **111**, 11494-11499.
7. G. Vijayaraghavan and K. J. Stevenson, *Langmuir : ACS J. surf. and colloids*, 2007, **23**, 5279-5282.
8. D. J. Guo and H. L. Li, *J. Electroanal. Chem.*, 2004, **573**, 197-202.
9. X. Li, W.-X. Chen, J. Zhao, W. Xing and Z.-D. Xu, *Carbon*, 2005, **43**, 2168-2174.
10. V. V. Pushkarev, N. Musselwhite, K. J. An, S. Alayoglu and G. A. Somorjai, *Nano Lett.*, 2012, **12**, 5196-5201.
11. L. Jia, D. A. Bulushev, O. Y. Podyacheva, A. I. Boronin, L. S. Kibis, E. Y. Gerasimov, S. Beloshapkin, I. A. Seryak, Z. R. Ismagilov and J. R. H. Ross, *J. Catal.*, 2013, **307**, 94-102.
12. R. Siburian, T. Kondo and J. Nakamura, *J. Phys. Chem. C*, 2013, **117**, 3635-3645.
13. F. Y. Li, Y. F. Li, X. C. Zeng and Z. F. Chen, *ACS Catal.*, 2015, **5**, 544-552.
14. S. Sun, G. Zhang, N. Gauquelin, N. Chen, J. Zhou, S. Yang, W. Chen, X. Meng, D. Geng, M. N. Banis, R. Li, S. Ye, S. Knights, G. A. Botton, T.-K. Sham and X. Sun, *Sci. Rep.*, 2013, **3**, doi:10.1038/srep01775.

15. L. Wang, S. Zhang, Y. Zhu, A. Patlolla, J. Shan, H. Yoshida, S. Takeda, A. I. Frenkel and F. Tao, *ACS Catal.*, 2013, **3**, 1011-1019.
16. A. C. Johansson, R. B. Yang, K. B. Haugshøj, J. V. Larsen, L. H. Christensen and E. V. Thomsen, *Int. J. Hydrogen Energy*, 2013, **38**, 11406-11414.
17. B. J. O'Neill, D. H. K. Jackson, J. Lee, C. Canlas, P. C. Stair, C. L. Marshall, J. W. Elam, T. F. Kuech, J. A. Dumesic and G. W. Huber, *ACS Catal.*, 2015, DOI: 10.1021/cs501862h, 1804-1825.
18. J. Lu, K.-B. Low, Y. Lei, J. A. Libera, A. Nicholls, P. C. Stair and J. W. Elam, *Nat. Commun.*, 2014, **5**. DOI: 10.1038/ncomms4264
19. Y. Lei, B. Liu, J. Lu, R. J. Lobo-Lapidus, T. Wu, H. Feng, X. Xia, A. U. Mane, J. A. Libera, J. P. Greeley, J. T. Miller and J. W. Elam, *Chem. Mat.*, 2012, **24**, 3525-3533.
20. J. Lu, B. Fu, M. C. Kung, G. Xiao, J. W. Elam, H. H. Kung and P. C. Stair, *Sci.*, 2012, **335**, 1205-1208.
21. X. Gu, W. Qi, X. Xu, Z. Sun, L. Zhang, W. Liu, X. Pan and D. Su, *Nanoscale*, 2014, **6**, 6609-6616.
22. P. G. Collins, K. Bradley, M. Ishigami and A. Zettl, *Sci.*, 2000, **287**, 1801-1804.
23. J. D. Kim, A. Pyo, K. Park, G. C. Kim, S. Lee and H. C. Choi, *B Korean Chem. Soc.*, 2013, **34**, 2099-2104.
24. C. N. R. Rao, A. Govindaraj and B. C. Satishkumar, *Chem. Commun.*, 1996, 1525-1526.
25. H. Ago, T. Kugler, F. Cacialli, W. R. Salaneck, M. S. P. Shaffer, A. H. Windle and R. H. Friend, *J. Phys. Chem. B*, 1999, **103**, 8116-8121.
26. S. Takenaka, T. Tsukamoto, H. Matsune and M. Kishida, *Catal. Sci. Technol.*, 2013, **3**, 2723-2731.
27. W. P. Deng, X. S. Tan, W. H. Fang, Q. H. Zhang and Y. Wang, *Catal. Lett.*, 2009, **133**, 167-174.
28. S. Akbayrak and S. Ozkar, *ACS App.l Mater. Interfaces*, 2012, **4**, 6302-6310.
29. W. Chen, J. Ji, X. Feng, X. Duan, G. Qian, P. Li, X. Zhou, D. Chen and W. Yuan, *J. ACS*, 2014, **136**, 16736-16739.
30. S. H. Sun, G. X. Zhang, N. Gauquelin, N. Chen, J. G. Zhou, S. L. Yang, W. F. Chen, X. B. Meng, D. S. Geng, M. N. Banis, R. Y. Li, S. Y. Ye, S. Knights, G. A. Botton, T. K. Sham and X. L. Sun, *Sci Rep-Uk*, 2013, **3**. DOI: 10.1038/srep01775
31. Z. Guo, C. Zhou, D. Shi, Y. Wang, X. Jia, J. Chang, A. Borgna, C. Wang and Y. Yang, *Appl. Catal. A: General*, 2012, **435–436**, 131-140.
32. X. F. Xie and L. Gao, *Carbon*, 2007, **45**, 2365-2373.
33. S. H. Liang, F. T. G. Bulgan, R. L. Zong and Y. F. Zhu, *J. Phys. Chem. C*, 2008, **112**, 5307-5315.
34. S. C. Wang, J. Yang, X. Y. Zhou and J. Xie, *Electron. Mater. Lett.*, 2014, **10**, 241-245.
35. X. L. Tong, Y. Qin, X. Y. Guo, O. Moutanabbir, X. Y. Ao, E. Pippel, L. B. Zhang and M. Knez, *Small*, 2012, **8**, 3390-3395.
36. Y.-T. Kim, K. Ohshima, K. Higashimine, T. Uruga, M. Takata, H. Suematsu and T. Mitani, *Angew. Chem. Int. Edit.*, 2006, **45**, 407-411.
37. Y. M. Liang, H. M. Zhang, H. X. Zhong, X. B. Zhu, Z. Q. Tian, D. Y. Xu and B. L. Yi, *J. Catal.*, 2006, **238**, 468-476.
38. S. Hu, L. P. Xiong, X. B. Ren, C. B. Wang and Y. M. Luo, *Int. J. Hydrogen Energy*, 2009, **34**, 8723-8732.
39. A. Allagui, M. Oudah, X. Tuaev, S. Ntais, F. Almomani and E. A. Baranova, *Int. J. Hydrogen Energy*, 2013, **38**, 2455-2463.
40. E. Yoo, T. Okata, T. Akita, M. Kohyama, J. Nakamura and I. Honma, *Nano Lett.*, 2009, **9**, 2255-2259.
41. D.-Q. Yang and E. Sacher, *J. Phys. Chem. C*, 2008, **112**, 4075-4082.

Text: one sentence, of maximum 20 words, highlighting the novelty of the work.
Colour graphic: maximum size 8cm x 4cm.

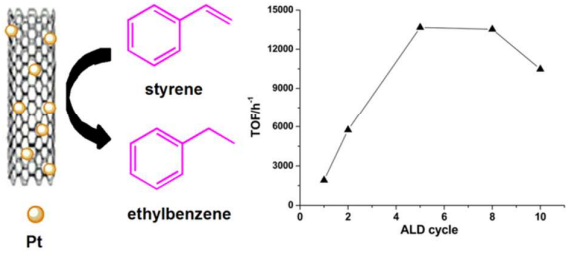

Pt sub-nanoparticles supported on carbon nanotubes prepared by atomic layer deposition exhibit unusual catalytic performance for styrene hydrogenation.